Model for Solid State Voltammetry of Zeolite-Associated Species

Antonio Doménech†

Departament de Química Analítica, Universitat de València, Dr. Moliner 50, 46100 Burjassot (València), Spain

Received: July 16, 2004; In Final Form: October 11, 2004

The electrochemical reduction/oxidation of zeolite-associated species is described from the model of Lovric and Scholz for redox conductive microcrystals and the model of Andrieux and Savéant for redox polymers. It is assumed that the reaction starts at the three-phase boundary between electrode, zeolite particle, and electrolyte. From this point, the reaction zone grows while electrons and charge-balancing cations diffuse perpendicularly along the zeolite. As a result, at short times, a Cottrell-type behavior, controlled by the diffusion of electrolyte countercations in the zeolite can be expected. At larger times, a thin-layer response in which electron hopping between adjacent redox sites acts as a rate-controlling step, should be operative. Experimental chronoamperometric data on Mn(salen)N_3 (salen = *trans*-(*R*,*R*)-1,2-bis(salicylideneamino)cyclohexane) associated with zeolite Y in contact with different MeCN electrolytes agree with these theoretical predictions. The diffusion coefficient of electrons across the zeolite was estimated to be as long as 2×10^{-11} cm^2/s whereas the diffusion coefficients of Li^+ and Et_4N^+ were found to be close to 1×10^{-9} cm^2/s. The thickness of the boundary electroactive zone of zeolite grains was estimated to be as long as 0.1−0.5 μm.

1. Introduction

Zeolites are crystalline aluminosilicates whose structure defines strictly periodic channels and cavities in which guest molecules can be trapped via ion exchange processes and ship-in-a-bottle synthesis. Incorporation of cationic guests into the crystalline framework of zeolites has claimed considerable attention because of the use of the resulting materials as heterogeneous catalysts for a number of reactions.[1,2]

The electrochemistry of such systems has been intensively studied in the past decade in view of the wide variety of applications of zeolite-modified electrodes and electrode-modified zeolites in electrocatalysis and electrochemical sensing.[3]

The electrochemistry of zeolite-associated species, however, has become controversial, the debate being focused on the extrazeolite/intrazeolite character of electrochemical processes occurring at zeolite-modified electrodes.[4−7] Description of this electrochemistry is complicated by the fact that the electron transfer process is accompanied by the ingress/egress of electrolyte cations into or from the adjacent electrolyte solution to maintain electroneutrality.

This matter was first treated by Gemborys and Shaw, who considered initially two possible electrochemical pathways: extrazeolitic and intrazeolitic.[8] A third mechanism, surface-mediated electron transfer, was considered by these authors[9] and Li and Mallouk,[10,11] whereas Calzaferri et al. distinguished between ion transport and electron transport intrazeolitic mechanisms.[12,13] From the works of Bessel and Rolison, it appears that the voltammetric response observed for zeolite-associated species reflects essentially the behavior of extrazeolite ion-exchanged molecules and/or those located in the more external "boundary" layer of the zeolite.[14] Data on the electrochemistry of zeolite-associated transition metal complexes[15] and reactive organic intermediates[16] provided results in agreement with such ideas. However, it appears that no detailed mechanisms for electron transfer processes are currently available.

The voltammetry of zeolite-asociated species can be compared with that of electroactive solids attached to inert electrodes. From the seminal works of Lamache and Bauer,[17] and Brainina and Vidrevich[18] on carbon paste electrodes, and the more recent studies of Scholz et al. on paraffin-impregnated graphite electrodes,[19,20] this field has experienced a considerable growth in the past decades, as described in extensive reviews.[21,22]

In this context, Lovric and Scholz[23,24] and Oldham[25] have recently developed theoretical models for explaining electron transfer processes involving nonconducting solids. In the more recent version formulated by Schröder et al.[26] electron transfer processes in a solid compound characterized by mixed ionic/electronic conductivity involve an initial reaction at the three-phase electrolyte/particle/electrode junction further extended via transport of electrons and charge-balancing cations in perpendicular directions. This scheme parallels that developed by Andrieux and Savéant[27] for describing electron transfer processes in redox polymers implying electron hopping between electroactive centers and the insertion of charge-balancing ions in the lattice of the solid. Such formulations can be applied for describing the electrochemistry of zeolite-associated species, in which electron transfer and ion transfer processes must occur.

The purpose of the current paper is to present an adaptation of such formulations for describing theoretically electron transfer processes in zeolite-supported species. The predictions of the model will be compared with previously reported voltammetric data for Mn(salen)N_3 (salen = *trans*-(*R*,*R*)-1,2-bis(salicylideneamino)cyclohexane) associated with zeolite Y[15] and additional chronoamperometric experiments.

2. Theory

2.1. Preliminary Considerations. Let us consider a zeolite particle immobilized on the surface of a conducting solid and in contact with an electrolyte. If the zeolite incorporates a

† E-mail: antonio.domenech@UV.es.

10.1021/jp046831z CCC: $27.50 © 2004 American Chemical Society
Published on Web 11/25/2004

cationic electroactive guest, X^+, it is in principle possible to obtain an electrochemical response from X^+ ions passing to the solution as a result of (i) the leaching of externally adsorbed X^+ and (ii) the exchange of X^+ with electrolyte cations, M^+:

$$X^+(z) + M^+(s) \rightarrow X^+(s) + M^+(z) \quad (1)$$

$$X^+(s) + e^- = X(s) \quad (2)$$

where (z) denotes the zeolite and (s) the solution phase.

Equations 1 and 2 describe the extrazeolite pathway in which the reduced species, X, egress from the zeolite to the solution phase.

In a number of cases, however, the electroactive species is so bulky as to avoid ion exchange processes described by eq 1. Encapsulation of such species, however, can be achieved through "ship-in-a-bottle" synthetic procedures from small precursor molecules.[28] Then, electron transfer processes may involve a concerted electron transport-ion transport along the zeolite bulk (intrazeolitic pathway). As a result, the reduced species remains attached to the zeolite framework. This can be represented as

$$X^+(z) + M^+(s) + e^- \rightarrow X(z) + M^+(z) \quad (3)$$

An intermediate situation can be proposed in which the electroactive species remains attached to the neighboring surface of the zeolite particles.

Prior results on the electrochemistry of bulky electroactive species attached to zeolites indicated that[15,16] (i) voltammetric responses in contact with size-excluded electrolyte countercations were clearly lower than those of the same materials in contact with non size-excluded countercations, (ii) in these last cases electroactive species represent a percentage of total entrapped compound typically between 0.5 and 1.5%, (iii) a dual voltammetric response was obtained, close to an ordinary thick-layer behavior at short times, but approaching a thin-layer behavior at relatively long times; additionally, (iv) electrocatalytic effects exerted by zeolite-associated species are significantly electrolyte-dependent.[29] All these features should be explained by any theoretical model dealing with the electrochemistry of zeolite-associated species.

2.2. Two-Dimensional Model for Boundary-Associated Electrochemsitry. Let us consider a three-phase system formed by an infinite electrode, the electrolyte, and an infinite particle of a solid containing localized redox sites but able to exchange mobile cations with the electrolyte. This situation is schematized in Figure 1. Here, the ($x > 0$, y, 0) plane represents the electrode/particle interface, the (0, y, z) plane is the electrolyte/particle interface, and the (x, y, 0) plane is the electrode/electrolyte interface.

It is assumed that, as in the case of redox polymers,[27] charge transfer across the solid involves electron hopping between adjacent localized redox sites, necessarily accompanied by the displacement of electron transfer inactive counterions so as to maintain electroneutrality. This can be represented as an insertion/electron transfer process that can be described by

$$A(z) + M^+(sol) + e^- \rightarrow B{-}M^+(z) \quad (4)$$

where A represents a the oxidized form of the immobile redox center, B its reduced form, and M^+ the mobile electroinactive electrolyte cations.

As studied by Andrieux and Savéant,[30] and Laviron,[31] as far as charge transport under a concentration gradient is concerned, this is formally equivalent to a diffusion obeying Fick's law of the immobile redox sites. The effect of an electric field is formally equivalent to migration of immobile redox centers obeying a modified version of the classical Nernst−Planck law.[32,33]

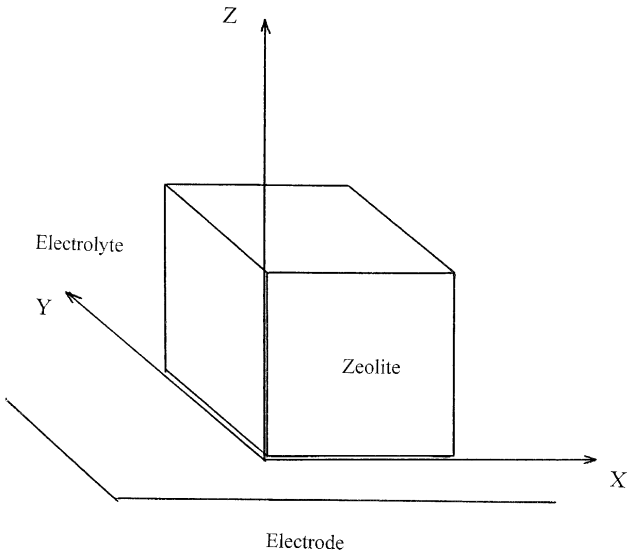

Figure 1. Schematics of the zeolite particle/electrode/electrolyte system.

The Lovric and Scholz model assumes explicitly that[24] (i) Charge-balancing cations M^+ can enter in the solid only through the (0, y, z) plane, starting in the vicinity of the (0, y, 0) line, i.e., in the three-phase junction. (ii) The flux of M^+ proceeds only in the x-direction. (iii) Electrons flow across the electrode/particle interface only in the z-direction. (iv) The concentrations of the oxidized and reduced centers (A/B) at the three-phase junction are thermodynamically governed.

Additionally, it will be assumed that the current/potential response is independent of the charge transfer kinetics at the electrode/zeolite, electrolyte/zeolite, and electrolyte/electrode interfaces and possible ohmic drops.[27]

If the electron transfer/cation insertion reaction described by eq 4 is thermodynamically governed, it describes an equilibrium that must satisfy the Nernst equation:

$$[A] = [B{-}M^+] \exp\left(\frac{nF(E - E_f)}{RT}\right) = [B{-}M^+]e^{\varphi} \quad (5)$$

where E_f is a formal electrode potential defined as

$$E_f = E^o + (RT/nF) \ln K + (RT/F) \ln[M^+] \quad (6)$$

In this equation, E^o is the standard potential of the redox couple A/B and K represents the equilibrium constant for the reaction of ion insertion described by eq 4.

In this model the equilibrium is initially established along the positive semiaxis y. The current is conducted over the crystal surface facing the electrolyte solution because M^+ ions flowing from the solution can compensate changes of charge from faradaic reactions. Here, electron transport proceeds via electron/ion hopping between immobile redox centers:

$$(A{-}M^+)_{siteI} + (B)_{siteII} \rightarrow (A)_{siteI} + (B{-}M^+)_{siteII} \quad (7)$$

This results in a net charge transfer that satisfies Fick's law of diffusion. Assuming that both ions and electrons are exchanged simultaneously and that no charge separation occurs one obtains[26]

$$\frac{\partial[\mathrm{B}-\mathrm{M}^+]}{\partial t} = D_x\frac{\partial^2[\mathrm{B}-\mathrm{M}^+]}{\partial x^2} = D_z\frac{\partial^2[\mathrm{B}-\mathrm{M}^+]}{\partial z^2} \quad (8)$$

In this equation D_x and D_z represent the diffusion coefficients in the x and z directions, respectively.

The instantaneous current verifies

$$di = nFD_x a dz\left(\frac{\partial[\mathrm{B}-\mathrm{M}^+]}{\partial x}\right)_{x=0} = nFD_x a dx\left(\frac{\partial[\mathrm{B}-\mathrm{M}^+]}{\partial z}\right)_{z=0} \quad (9)$$

where a and b represent the length of the crystal/electrode and the crystal/electrolyte junctions, respectively.

Assuming that the time experiment is sufficiently short to ensure that the diffusion−migration layer thickness is small as compared to the solid thickness, the problem can be described in terms of the semi-infinite boundary conditions:

$$t = 0: \quad [\mathrm{A}] = c_\mathrm{o} \qquad [\mathrm{B}-\mathrm{M}^+] = 0 \quad (10)$$

$$t > 0, x \to \infty: \quad [\mathrm{A}] \to c_\mathrm{o} \qquad [\mathrm{B}-\mathrm{M}^+] \to 0 \quad (11)$$

$$z \to \infty: \quad [\mathrm{A}] \to c_\mathrm{o} \qquad [\mathrm{B}-\mathrm{M}^+] \to 0 \quad (12)$$

$$x \geq 0, z \geq 0: \quad [\mathrm{A}] + [\mathrm{B}-\mathrm{M}^+] = c_\mathrm{o} \quad (13)$$

$$x = 0, z = 0: \quad [\mathrm{A}] = [\mathrm{B}-\mathrm{M}^+]\mathrm{e}^{-\varphi} \quad (14)$$

Here, the isoconcentration profiles are straight lines that, for a three-dimension model, correspond to plane surfaces. The concentration of the reduced form satisfies[26]

$$[\mathrm{B}-\mathrm{M}^+] = \frac{c_\mathrm{o}}{1+\mathrm{e}^{\varphi}}\,\mathrm{erfc}\left\{\frac{1}{2t^{1/2}}\left(\frac{x}{2D_x^{1/2}} + \frac{z}{2D_z^{1/2}}\right)\right\} \quad (15)$$

These equations provide the basis for describing the intrazeolite electrochemistry of zeolite-associated species, i.e., when cation diffusion and electron hopping may be operative in the zeolite bulk. However, the fact that only ca. 1% of entrapped electroactive molecules are electroactive suggests that at least electron conductivity is significantly hindered across the zeolite particles. This assumption is also consistent with data concerning electron diffusion and ion diffusion in redox polymers.[27]

Numerical simulations using finite diference methods developed by Schröder et al.,[26] yield

$$i = nFc_\mathrm{o}\left(\frac{1}{1+\mathrm{e}^{-\varphi}}\right)\left[b\left(\frac{\Delta x_\mathrm{o} D_z^{1/2} + \Delta z_\mathrm{o} D_x^{1/2}}{2\pi^{1/2}t^{1/2}}\right) + (D_x D_z)^{1/2}\right] \quad (16)$$

where Δx_o and Δz_o are the size of the three-phase junction boxes in which the crystal is divided for applying simulation procedures and b represents the length of the electrolyte/zeolite junction. This equation predicts a Cottrell-like behavior incorporating an additional time-independent term.

With this regard, it is important to recognize that there is redox conductivity even (i) if the solid particle cannot be penetrated by the ions M^+, i.e., if $D_x = 0$, and (ii) if the redox propagation reaction described by eq 7 cannot take place, i.e., when $D_z = 0$.

For our purposes, the relevant point to emphasize is that there is possibly a redox conductivity even if electron transfer processes cannot proceed in the bulk of the zeolite ($D_z = 0$). Then, the reaction remains surface confined and the chronoamperometric current is in principle equivalent to that of an ordinary Cottrell response.

For zeolite electrochemistry, one can in principle assume that the diffusion of electrons is clearly slower than the diffusion of cations. Accordingly, assuming that $D_x \gg D_z$, eq 16 becomes

$$i = nFc_\mathrm{o}\left(\frac{1}{1+\mathrm{e}^{-\varphi}}\right)\left[\frac{S_\mathrm{eff} D_x^{1/2}}{2\pi^{1/2}t^{1/2}} + b(D_x D_z)^{1/2}\right] \quad (17)$$

where S_eff is an effective area. It should be noted that S_eff is a rather intangible quantity because in typical experiments at zeolite-modified electrodes, there is an assembly of immobilized microcrystals whose shapes and sizes distribution must necessarily influence the electrochemical response.

A second approach can be obtained upon the assumption that the diffusion of the electrons across the zeolite is limited to a small, boundary, region of thickness δ near the zeolite/electrode interface. This situation corresponds to the boundary condition

$$t > 0, z = \delta: \quad (\partial[\mathrm{B}-\mathrm{M}^+]/\partial z)_{z=\delta} = 0 \quad (18)$$

In its more simplified version, this problem refers to well-known thin-layer electrochemistry. The chronoamperometric current can be expressed as[34]

$$i = \frac{4nFSD_z c_\mathrm{o}}{\delta}\left(\frac{1}{1+\mathrm{e}^{-\varphi}}\right)\sum_{j=0}^{\infty}\left[\frac{(2j-1)^2\pi^2 D_z t}{\delta^2}\right] \quad (19)$$

In this equation, S represents the area of the zeolite in contact with the electrode surface. At the first-order approximation ($j = 0$), in experiments at a given potential, plots of ln i vs t must give straight lines of slope $\mathrm{SL} = \pi^2 D_z/\delta^2$ and y-axis intercept $\mathrm{OO} = \ln(4nFSDc_\mathrm{o}/\delta)$. Accordingly, the thickness of the thin layer region can be calculated as $\delta = \pi^2 \exp(\mathrm{OO})/(\mathrm{SL})4nFSc_\mathrm{o}$.

As pointed out by Schröder et al.,[26] the reaction at the three-phase junction only initially determines the course of the electrochemical process. This initial step involves the exhaustive conversion described by eq 4 along the three-phase junction. After this, the electrochemical process is determined by the diffusion of cations and electrons through the zeolite/electrolyte and zeolite/electrode interfaces. As a result, equations for planar diffusion hold.

2.3. Refinements. First, the Lovric−Scholz model can be developed, introducing the more realistic assumptions that (i) the diffusion of M^+ ions can take place in the x- and y-directions (three-dimensional model) and (ii) the crystal has a finite size. Numerical simulations using finite difference methods demonstrate that at short times quasi semi-infinite conditions apply to the diffusion of both electrons and cations and current/time curves approaches:[26]

$$i = nFc_\mathrm{o}\left(\frac{1}{1+\mathrm{e}^{-\varphi}}\right)\left[p\left(\frac{\Delta x_\mathrm{o} D_z^{1/2} + \Delta z_\mathrm{o} D_x^{1/2}}{2\pi^{1/2}t^{1/2}}\right) + (D_x D_z)^{1/2} - 4D_x(2D_z t)^{1/2}\right] \quad (20)$$

where p represents the perimeter of the three-phase junction. Isotropy is assumed with respect to the diffusion of electrolyte cations through the zeolite, i.e.: $D_x = D_y$.

Equation 20 predicts a current vs time dependence similar to that described by eq 16 but incorporating an additional time-dependent term. This last is independent of the length of the

three-phase junction, being interpreted as a result of the "edge effect" associated with cation diffusion near the corners of the particle.[26]

Assuming, as before, that the diffusion of electrons is clearly slower than the diffusion of cations, at short times, the third term of eq 20 vanishes and, assuming that $D_x \gg D_z$, this equation reduces to eq 17 by inserting the perimeter p of the three-phase junction in the place of b.

If the diffusion of cations is fast compared to the diffusion of electrons, after exhaustive conversion of the oxidized centers A along the zeolite/electrode interface, the electron diffusion becomes rate-determining and chronoamperometric curves can be described by[34]

$$i = \frac{2nFSD_z c_o}{h}\left(\frac{1}{1+e^{-\varphi}}\right)\sum_{j=0}^{\infty}\exp\left[\frac{(2j-1)^2\pi^2 D_z t}{4h^2}\right] \quad (21)$$

where h represents the crystal height.

Regardless of geometrical factors, this equation is formally identical to eq 19 and enables a direct determination of D_z and h from current/time curves. At the first-order approximation ($j = 0$), plots of ln i vs t must give straight lines of slope SL $= \pi^2 D_z/4h^2$ and ordinate at the origin OO $= \ln(2nFSD_z c_o/h)$. Accordingly, the thickness of the electroactive layer can be calculated as $h = \pi^2 \exp(\mathrm{OO})/(\mathrm{SL})8nFSc_o$, and the vertical diffusion coefficient can be obtained as $D_z = 4h^2(\mathrm{SL})/\pi^2$.

A second set of refinements arises from the detailed consideration of the mechanism of electron hopping. On studying polymeric films, Kaufman and Engler originally proposed that charge propagates between redox sites anchored to the polymeric chains by means of electron hopping between adjacent oxidized and reduced sites.[35] Following the earlier analyses of Dahms,[36] and Ruff and Friedrich,[37] the experimentally observed diffusion coefficient for one-half of a redox couple in homogeneous solution, D, in the presence of a second-order self-exchange reaction, can be expressed as

$$D = D_o + \pi k_{ex} c_o \rho/4 \quad (22)$$

where D_o is the diffusion coefficient in the absence of self-exchange, c_o is again the sum of the concentrations of the oxidized and reduced forms of the redox couple, k_{ex} is the exchange rate constant, and ρ is the distance between the centers of the reactants when the electron transfer occurs.

This equation is valid in the case in which the ratio of the concentration gradients of the oxidized and reduced forms of the reactant are everywhere equal to -1, a condition that commonly applies in electrochemical experiments.[38] A more recent approach based upon the kinetic Ising model has been recently reported by Denny and Sangaranarayanan.[39]

An additional set of refinements can be derived by considering kinetic complications arising in the electron transfer at the zeolite/electrode interface and the cation transfer at the zeolite/electrolyte interface. Further, the electron transfer/interchange process (eq 4) may be under kinetic control, thus resulting in a nonreversible electrochemistry. Finally, it should be noted that several factors (ion pairing, etc.) may cause Fick's equations to fail, as discussed for redox polymers.[27]

3. Experimental Section

The precursor Y zeolite-encapsulated Mn(salen)$^+$ complex was prepared by condensation of *trans*-(*R*,*R*)-1,2-diaminocyclohexane and salicylaldehyde in Mn^{2+}-exchanged zeolite Y (0.48% Mn^{2+}), as previously described.[40] The Mn(salen)N_3 complex was prepared by treatment with trimethylsilyl azide of the parent zeolite-associated Mn(salen)$^+$ complex and intrazeolite condensation with *trans*-(*R*,*R*)-1,2-diaminocyclohexane. After removal of the excess ligand by Soxhlet extraction in CH_2Cl_2 for 8 h, the encapsulated complex was ion exchanged with an aqueous 1 M NaCl solution for 12 h. Spectrochemical characterization of the resulting material, as already reported,[41,42] indicated that a "clean" synthesis of Mn(salen)N_3 units within the supercages of zeolite Y occur. The concentration of Mn(salen)N_3 in the zeolite was calculated to be 2.2×10^{-4} mol/cm^3, corresponding to ca. 1 Mn center for each 5 zeolite supercages.

Commercially available Paraloid B72, an ethyl acrylate (70%)−methyl acrylate (30%) copolymer (P[EMA/MA]) was selected for polymer-film electrode preparation because of its mechanical stability and ability to form porous films able to adhere the zeolite microparticles to the electrode surface.

Polymer-film sample-modified electrodes were prepared, as previously described,[15,16] by transferring a few microliters (typically 50 μL) of a dispersion of the solid (10 mg) in acetone (5 mL) to the surface of freshly polished platinum (geometrical area 0.018 cm^2) and glassy carbon (GCE, geometrical area 0.071 cm^2) electrodes and allowing the coating to dry in air. After the electrode surface was air-dried, one drop of a solution of the acrylic resin (1%) in acetone was added and the modified electrode was again air-dried. The coatings contained 0.00015 $\pm$ 0.00005 g of zeolite. Examination by scanning electron microscopy indicated that the zeolite deposit consisted of a uniform distribution of aggregates of particles 5−10 μm size.[15] Blank experiments were performed using electrodes modified with pristine, non-Mn(salen)N_3-containing, zeolite Y.

Chronoamperograms and cyclic voltammograms (CAs and CVs, respectively) were performed with a BAS CV50W equipment. A standard three-electrode arrangement was used with a platinum auxiliary electrode and a AgCl (3 M NaCl)/Ag reference electrode, separated from the bulk solution by a salt bridge, in a cell thermostated at 298 K. MeCN solutions of $LiClO_4$ (Aldrich), Et_4NClO_4 (Acros), and Bu_4NPF_6 (Fluka) were used as supporting electrolytes.

4. Results and Discussion

4.1. Chronoamperometric Responses. As previously reported, reduction of zeolite-associated Mn(salen)N_3 ions occurs via a reversible one-electron process at an equilibrium potential close to −0.25 V vs AgCl/Ag in MeCN electrolytes.[15] Application of a constant potential of −0.45 V at zeolite-modified electrodes immersed into different electrolytes provides well-defined chronoamperometric curves, as depicted in Figure 2. Corrected curves were obtained by subtracting the CA recorded at an electrode modified with pristine zeolite Y, from those obtained at electrodes modified by Mn(salen)N_3-containing Y zeolite. Remarkably, the currents in contact with Et_4N^+/MeCN and Li^+/MeCN electrolytes were similar, but clearly larger than those in contact with Bu_4N^+/MeCN.

In Figure 3 the corresponding Cottrell plots of i vs $t^{-1/2}$ are shown. At times less than 10 s, an excellent linearity (correlation coefficients between 0.9997 and 1.0000) was obtained in all cases, as denoted by statistical parameters summarized in Table 1. At times longer than 10 s, however, experimental data diverge from linearity, especially in the case of Li^+/MeCN and Et_4N^+/MeCN electrolytes.

For Li^+/MeCN and Et_4N^+/MeCN electrolytes, CA data at times larger than 30−40 s diverge clearly from the foregoing Cottrell behavior. These data fit well with the thin-layer response

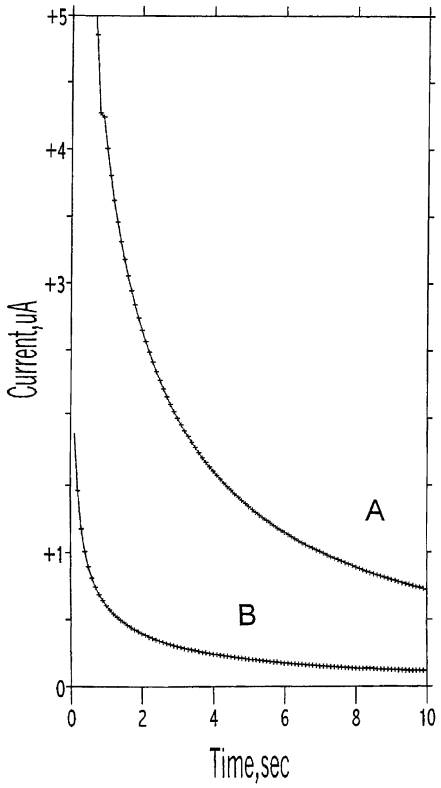

Figure 2. Chronoamperograms at a fixed potential of −0.45 V for zeolite Y-associated Mn(salen)N_3 electrodes immersed into (A) 0.10 M Et_4NClO_4/MeCN and (B) 0.10 M Bu_4NPF_6/MeCN. Current−time curves after subtraction of blank CAs recorded at electrodes modified with pristine zeolite.

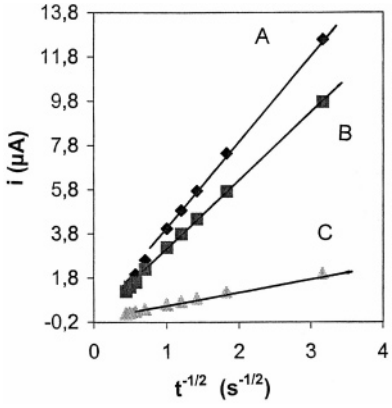

Figure 3. Cottrell plots of i vs $t^{-1/2}$ from CAs at a fixed potential of −0.45 V for zeolite Y-associated Mn(salen)N_3 electrodes immersed into (A) 0.10 M Et_4NClO_4/MeCN, (B) 0.10 M $LiClO_4$/MeCN, and (C) 0.10 M Bu_4NPF_6/MeCN.

described by eq 21, as can be seen in Figure 4, in which ln i vs t plots are shown. Statistical data summarized in Table 2 indicate that an excellent linearity was obtained for such electrolytes (correlation coefficients between 0.9997 and 1.0000).

This dual thick-layer/thin-layer response has been obtained in different zeolite systems using different voltammetric techniques.[15,16] A situation similar has been described by Daum et al. for redox polymers.[43]

4.2. Boundary Thickness and Electron Diffusion. As previously noted, long-time CA data (t > 40 s) fit with a thin-layer current/time dependence that permits a direct estimate of the coefficient of diffusion for electrons and the thickness of the electron diffusion layer. Pertinent data are shown in Table 1.

TABLE 1: Statistical Parameters from CA Curves Recorded for Electrodes Modified with Mn(salen)N_3-Containing Y Zeolite Immersed into Et_4NClO_4/MeCN, $LiClO_4$/MeCN, and Bu_4NPF_6/MeCN Electrolytes (All in Concentrated 0.10 M) at Times between 0 and 10 s[a]

electrolyte cation	Cottrell slope	Cottrell ordinate	r	D_x (cm²/s)[b]	D_x (cm²/s)[c]
Et_4N^+	3.901	0.270	0.9999	1.06×10^{-9}	1.30×10^{-9}
Et_4N^+	3.884	0.307	1.0000	2.02×10^{-9}	1.29×10^{-9}
Et_4N^+	3.935	0.183	0.9999	7.17×10^{-10}	1.33×10^{-9}
Li^+	3.040	0.159	1.0000	5.41×10^{-10}	7.92×10^{-10}
Li^+	3.026	0.192	1.0000	7.89×10^{-10}	7.85×10^{-10}
Li^+	3.050	0.156	0.9999	5.21×10^{-10}	7.97×10^{-10}
Bu_4N^+	0.627	0.004	0.9995	3.42×10^{-13}	4.11×10^{-11}
Bu_4N^+	0.624	0.017	0.9995	5.35×10^{-12}	3.38×10^{-11}
Bu_4N^+	0.692	−0.089	0.9997		3.34×10^{-11}

[a] Applied potential −450 mV vs AgCl (3 M NaCl)/Ag. [b] Diffusion coefficients calculated from eq 21 by inserting $p = 72$ cm; $c_o = 2.2 \times 10^{-4}$ mol/cm³. [c] Id. calculated from eq 17 by taking $S_{eff} = 0.018$ cm².

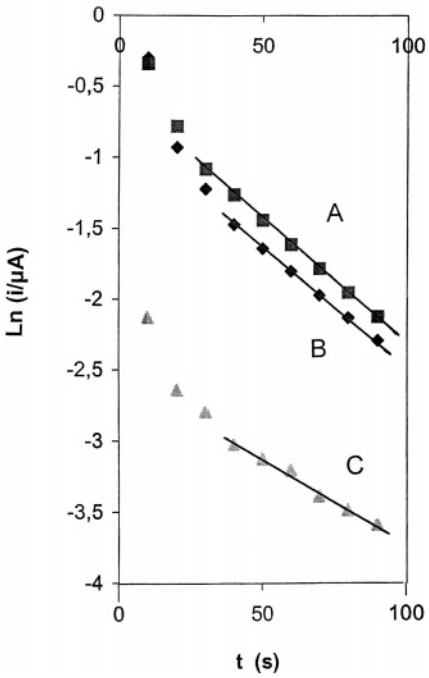

Figure 4. ln i vs t plots from CAs at a fixed potential of −0.45 V for zeolite Y-associated Mn(salen)N_3 electrodes immersed into (A) 0.10 M Et_4NClO_4/MeCN, (B) 0.10 M $LiClO_4$/MeCN, (C) 0.10 M Bu_4NPF_6/MeCN.

Assuming that the deposit of zeolite grains is equivalent to a uniform layer whose area equals the geometrical area of the basal electrode, the mean thickness of the studied deposits was ca. 35 μm. Then, the thickness of the electroactive layer in contact with the electrode surface can be estimated (i) from CA data using the prior modelization and (ii) from the net charge passed in voltammetric experiments calculated from the area under voltammetric peaks.

In this second case, previously reported data,[15] provided, in contact with Et_4N^+/MeCN and Li^+/MeCN electrolytes, a percentage of electroactive Mn(salen)N_3 of 0.7% with respect to total zeolite-encapsulated complexes. Assuming that electroactive complexes are located along a boundary layer near the zeolite−electrode interface, the thickness of this layer can be calculated as long as 0.2 μm, i.e., a 0.6% of the thickness of the zeolite deposit.

For Li^+/MeCN and Et_4N^+/MeCN electrolytes, the thin-layer response fits to eq 21, from which the values of the coefficient

TABLE 2: Statistical Parameters from CA Curves Recorded for Electrodes Modified with Mn(salen)N_3-Containing Y Zeolite Immersed into Et_4NClO_4/MeCN, $LiClO_4$/MeCN, and Bu_4NPF_6/MeCN Electrolytes (All in Concentrated 0.10 M) at Times between 30 and 80 s[a]

electrolyte	thin-layer slope	thin-layer ordinate	r	δ (μm)	D_z (cm^2/s)
Et_4N^+	−0.0164	−0.820	0.9997	0.87	5.03×10^{-11}
Et_4N^+	−0.0174	−1.059	0.9998	0.64	2.89×10^{-11}
Et_4N^+	−0.0170	−0.962	0.9997	0.73	3.67×10^{-11}
Li^+	−0.0176	−1.250	1.0000	0.53	2.00×10^{-11}
Li^+	−0.0179	−1.237	1.0000	0.52	1.96×10^{-11}
Li^+	−0.0239	−1.016	0.9997	0.49	2.32×10^{-11}
Bu_4N^+	−0.0116	−2.542	0.983	0.22	2.25×10^{-12}
Bu_4N^+	−0.0100	−2.620	0.991	0.24	2.33×10^{-12}
Bu_4N^+	−0.0135	−2.317	0.975	0.24	2.33×10^{-12}

[a] Applied potential −450 mV vs AgCl (3 M NaCl)/Ag. Diffusion coefficients and thin-layer thickness calculated from eq 20 by inserting $S = 0.018$ cm^2; $c_o = 2.2 \times 10^{-4}$ mol/cm^3.

of diffusion of electrons, D_z, and the thickness of the boundary "electroactive" layer, h, can be calculated. The obtained results are summarized in Table 2. Applying eq 21 to such CA data, similar values of the electroactive layer thickness for zeolite Y-associated Mn(salen)N_3 in Et_4N^+/MeCN and Li^+/MeCN were found, ranging from 0.5 to 0.8 μm. For Bu_4N^+/MeCN the thickness was 0.2 μm. When the studied zeolite-modified electrodes are considered a uniform distribution of grains, one finds that the penetration to a uniform zeolite layer is between 1.5 and 2.5% of the entire zeolite layer for Et_4N^+/MeCN and Li^+/MeCN electrolytes. These values, however, must be regarded with caution: because the zeolite crystallites are 1−10 μm in size, these data suggest that the electroactive layer is extended over a significant portion of the crystallites.

Consistent with theory, the value of D_z is almost identical for both electrolytes and close to that calculated for electron diffusion in redox polymers.[27,43] This value is ca. 100 times lower than those calculated for the diffusion of electrolyte cations in the zeolite pore/channel system (vide infra).

In contrast, CA data for Bu_4N^+/MeCN do not fit with eq 21. As shown in Table 2, ln i vs t plots provide poor correlation coefficients (0.97−0.99) in this case. Although these values cannot be considered representative, the estimated value of D_z is ca. 10 times lower than the values calculated for Li^+/MeCN and Et_4N^+/MeCN electrolytes.

It should be noted that electron hopping is uneasy in zeolites, in which large separation between redox centers confined in supercages exists. However, to any extent, electron hopping between adjacent redox centers can occur. Following the literature, significant electronic interactions between adjacent $Ru(bpy)_3^{2+}$ encapsulated into zeolite Y occur, as revealed by spectrocscopic data.[44]

Current data confirm the idea that electron hopping is effectively confined to a small boundary layer of the zeolite particles. However, the values of the thickness of that layer, h, estimated from the area under voltammetric peaks differ from those calculated, using eq 21, from chronoamperometric data. There are discrepancies that can be attributed to the nature of the assumptions made for calculations. First of all, the modified electrode is regarded as a uniform zeolite deposit, avoiding an account for the shape and size distribution of the zeolite particles. Then, the use of the geometrical area of the electrode into the calculations is only a rough approximation. Additionally, it should be noted that the concentration of electroactive Mn(salen)N_3 is explicitly inserted into eq 21. The values of h estimated from CA data in Table 2 were derived by taking the mean concentration of complex in the zeolite bulk, 2.2×10^{-4} mol/cm^3. However, it is known that the distribution of guest molecules into the zeolite crystals is not uniform, being larger just at the external zone of the crystals. Thus, Lainé et al. have recently reported detailed data on zeolite Y-associated $Ru(bpy)_3^{2+}$ showing that, for high ruthenium loadings, there is a clear tendency of $Ru(bpy)_3^{2+}$ to accumulate toward the surface of the zeolite microparticles instead of a random distribution in the bulk.[45]

Thus, following eqs 21 and 22, if the effective concentration of electroactive species increases, the thickness of the electroactive layer decreases. Accordingly, for an effective boundary concentration of Mn(salen)N_3 5 times larger (all supercages occupied) than its mean value in the zeolite, the values of h calculated from eq 21 agree well with those estimated from the area under voltammetric peaks without account of concentration. Then the thickness of the electroactive layer becomes ca. 0.10 μm, clearly lower than the crystallite size (1−10 μm).

4.3. Cation Diffusion. As previously indicated, experimental CA data at $t < 30$ s, are close to a Cottrell-type behavior. In particular, data at $t < 1$ s exhibit an excellent fit with a linear variation of i vs $t^{-1/2}$ with correlation coefficients of 1.0000 (see Table 1).

Such data can be correlated with eq 20 by neglecting the last time-dependent term. Using this assumption, plots of i vs $t^{-1/2}$ must give a straight line of y-axis intercept $nFc_0p(D_xD_z)^{1/2}$. Statistical parameters for linear i vs $t^{-1/2}$ correlations are summarized in Table 1. By inserting the values of D_z previously calculated, one can obtain the values of D_x provided that the perimeter of the three-phase junction is known. To estimate this last parameter, a model for the shape and size distribution of zeolite particles is needed.

In agreement with secondary electron microscope (SEM) images,[15] the existing zeolite deposits in modified electrodes used here can in principle be described in terms of a set of cuboids of edge between 5 and 10 μm forming irregular aggregates. The number of cuboids, N, can in principle be estimated as the quotient between the electrode area, S, and a^2, a being the edge of the cuboids. Taking $S = 0.018$ cm^2 and $a = 10$ μm, one obtain $N = 1.8 \times 10^4$ cuboids. Then, the perimeter of the three phase junction can be estimated as $p = 4Na$, providing a value of 72 cm.

Accordingly, D_x can be calculated from the ordinate at the origin, OO, of i vs $t^{-1/2}$ plots as $D_x = (OO)^2/n^2F^2c_o^2p^2D_z$. The values of the diffusion coefficient for Et_4N^+ and Li^+ were similar but at least 200 times larger than that for Bu_4N^+. Diffusion coefficients of Et_4N^+ and Li^+ were ca. 100 times larger than the diffusion coefficient of electrons, D_z.

Attempting to test the self-consistency of the current modelization, a second set of values of D_x were calculated, using eq 17, from the slope of i vs $t^{-1/2}$ plots as $D_x = 4\pi(SL)^2/n^2F^2c_o^2S_{eff}^2$. This requires the use of a value of the effective area, S_{eff}. To estimate S_{eff}, one can assume that the modified electrode is formed by a uniform layer of cuboids exposed to the electrolyte solution. Using this approach, and considering that cation diffusion is restricted to vertical faces of cuboids, the maximum exposed area equals to $4Na^2$. If a dense array of cuboids exists, as suggested by SEM images, a more realistic approach can be to take $S_{eff} = Na^2 = 0.018$ cm^2. The values of D_x, calculated from the slope of i vs $t^{-1/2}$ plots are shown in Table 1. These values are close to those calculated from the ordinate at the origin of such Cottrell plots.

Chronoamperometric data for zeolite Y-associated Mn(salen)N_3 in contact with $LiClO_4$/MeCN and Et_4NClO_4/MeCN elec-

trolytes can be interpreted at the light of the current scheme as a result of cation diffusion and electron diffusion in perpendicular directions.

The results for Bu_4N^+/MeCN can in principle be interpreted on the basis of the recognized size-excluded character of Bu_4N^+ ions. It is known that Li^+ and Et_4N^+ cations, but not the Bu_4N^+ one, can enter into the faujasite pore/channel system.[8,46] Thus, the response observed in Bu_4NPF_6/MeCN can be described within the above scheme assuming that a certain degree of ion transport is possible at least in a very shallow zeolite boundary.

Faujasite Y-zeolite is composed of supercages whose internal diameter is ca. 13 Å connected to one another, in a tetrahedral arrangement, through 7.4 Å windows to form a three-dimensional network. The unit cell, whose volume falls in the range 14.90−15.35 nm^3 is composed by eight supercages, containing approximately 250 molecules of water and 56 Na^+ ions distributed over the free volume of large supercages and smaller β-cages.[47,48] Although the "size" of Bu_4N^+ ions is larger to ingress across zeolite windows, it has been reported that owing the flexibility of such molecule, a certain degree of ion exchange is possible.[49] Otherwise, defect surface sites may permit the pass of bulky Bu_4N^+ ions into the zeolite framework. This scheme appears to be consistent with the obtained data on considering that (i) the estimated diffusion coefficient for electrons (see Table 2) in Bu_4N^+/MeCN is 10 times lower than that calculated in Et_4N^+/MeCN and Li^+/MeCN and (ii) the diffusion coefficient of Bu_4N^+ ions into the zeolite is above 20 times lower than those calculated for Et_4N^+/MeCN and Li^+/MeCN. Additionally, the redox conductivity in the presence of Bu_4N^+ can be attributed to species adsorbed on the external surface of the zeolite grains passing to the solution phase. The diffusion coefficients of Li^+ and Et_4N^+ in the zeolite were found to be similar, close to 1×10^{-9} cm^2/s. This similarity can be attributed to the fact that metal ions are accompanied by solvent molecules when diffusing through zeolite pores,[49,50] and then the effective radius of Li^+ and Et_4N^+ should be comparable.

5. Final Considerations

The electrochemistry of bulky electroactive species encapsulated into zeolites can be described on the basis of the model of Lovric−Scholz and Oldham for redox conductive microcrystals and that of Andrieux and Savéant for redox polymers. In this scheme, the reaction is initiated at the three-phase junction between the crystal, the electrode, and the electrolyte solution, from which it proceeds via diffusion of electrolyte charge-balancing cations across the zeolite pore/channel system, and the diffusion of electrons via electron hopping between immobile redox centers. Assuming reversibility and that the diffusion of ions and electrons takes place in perpendicular directions, two different electrochemical responses can be predicted: at short times, semi-infinite diffusion conditions hold and a thick-layer, Cottrell-type behavior appears; at long experimentation times, a thin-layer response is expected.

Chronoamperometric data on zeolite Y-associated Mn(salen)-N_3 complex in contact with Et_4N^+/MeCN and Li^+/MeCN electrolytes agree well with the results expected from the model. The diffusion coefficients for such cations in the zeolite are close to 1×10^{-9} cm^2/s whereas the coefficient of diffusion of electrons is ca. 2×10^{-11} cm^2/s. These results are consistent with the idea that the effective propagation of the electron transfer reactions is limited to a small boundary zone of the zeolite grains. The thickness of that boundary layer is calculated to be as long as ca. 0.2−0.5 μm, corresponding to a small portion (<2%) of the zeolite grains. The dependence of voltammetric data on the concentration of supporting electrolyte is also in agreement with the predictions of the model.

At the expense of future developments of that model and more detailed experimental studies dealing with the influence of the size and shape distribution of zeolite particles in the modified electrode, it appears that the described model provides a satisfactory interpretation of the electrochemistry of zeolite-associated species on the basis of a redox solid-state conductivity.

Acknowledgment.

Financial support of the Generalitat Valenciana I+D Project GV04B-197 is gratefully acknowledged.

References and Notes

(1) Rolison, *D. R. Stud. Surf. Sci. Catal.* **1994**, *85*, 543.
(2) Dutta, P. K.; Ledney, M. *Prog. Inorg. Chem.* **1997**, *44*, 209.
(3) Rolison, D. R.; Bessel, C. A. *Acc. Chem. Res.* **2000**, *33*, 737.
(4) Baker, M. D.; Senaratne, C.; McBrien, M. *J. Phys. Chem.* **1995**, *99*, 12367.
(5) Li, J.-W.; Pfanner, K.; Calzaferri, G. *J. Phys. Chem.* **1995**, *99*, 12368.
(6) Bedioui, F.; Devynck, J.; Balkus Jr., K. J. *J. Phys. Chem. B* **1996**, *100*, 8607.
(7) Senaratne, C.; Baker, M. D.; Zhang, J.; Bessel, C. A.; Rolison, D. R. *J. Phys. Chem. B* **1996**, *100*, 8610.
(8) Gemborys, H. A.; Shaw, B. R. *J. Electroanal. Chem.* **1986**, *208*, 95.
(9) Shaw, B. R.; Creasy, K. E.; Lancycjiki, C. J.; Sargeant, J. A.; Tirhado, M. *J. Electrochem. Soc.* **1988**, *135*, 869.
(10) Li, Z.; Mallouk, T. E. *J. Phys. Chem.* **1987**, *91*, 643.
(11) Li, Z.; Wang, C. M.; Persaud, L.; Mallouk, T. E. *J. Phys. Chem.* **1988**, *92*, 2592.
(12) Li, J.-W.; Calzaferri, G. *J. Electroanal. Chem.* **1994**, *377*, 163.
(13) Li, J.-W.; Pfanner, K.; Calzaferri, G. *J. Phys. Chem.* **1995**, *99*, 2119.
(14) Bessel, C. A.; Rolison, D. R. *J. Phys. Chem. B* **1997**, *101*, 1148.
(15) Doménech, A.; Formentín, P.; García, H.; Sabater, M. J. *J. Phys. Chem. B* **2002**, *106*, 574.
(16) Doménech, A.; García, H.; Alvaro, M.; Carbonell, E. *J. Phys. Chem. B* **2003**, *107*, 3040.
(17) Lamache, M.; Bauer, D. *Anal. Chem.* **1979**, *51*, 1320.
(18) Brainina, K.h. Z.; Vidrevich, M. B. *J. Electroanal. Chem.* **1981**, *121*, 1.
(19) Scholz, F.; Nitschke, L.; Henrion, G. *Naturwiss.* **1989**, *76*, 71.
(20) Scholz, F.; Nitschke, L.; Henrion, G.; Damaschun, F. *Naturwissenschaften* **1989**, *76*, 167.
(21) Scholz, F.; Meyer, B. *Electroanalytical Chemistry, A Series of Advances* Bard, A. J., Rubinstein, I., Eds.; Marcel Dekker: New York, 1998; Vol. 20, pp 1−87.
(22) Grygar, T.; Marken, F.; Schröder, U.; Scholz, F. *Collect. Czech. Chem. Commun.* **2002**, *67*, 163.
(23) Lovric, M.; Scholz, F. *J. Solid State Electrochem.* **1997**, *1*, 108.
(24) Lovric, M.; Scholz, F. *J. Solid State Electrochem.* **1999**, *3*, 172.
(25) Oldham, K. B. *J. Solid State Electrochem.* **1998**, *2*, 367.
(26) Schröder, U.; Oldham, K. B.; Myland, J. C.; Mahon, P. J.; Scholz, F. *J. Solid. State Electrochem.* **2000**, *4*, 314.
(27) Andrieux, C. P.; Savéant, J. M. *J. Phys. Chem.* **1988**, *92*, 6761.
(28) Scaiano, J. C.; García, H. *Acc. Chem. Res.* **1998**, *32*, 783.
(29) Doménech, A.; García, H.; Casades, I.; Esplá, M. *J. Phys. Chem. B*, in press.
(30) Andrieux, C. P.; Savéant, J.-M. *J. Electroanal. Chem.* **1980**, *111*, 377.
(31) Laviron, E. *J. Electroanal. Chem.* **1980**, *112*, 1.
(32) Savéant, J.-M- *J. Electroanal. Chem.* **1986**, *201*, 211.
(33) Savéant, J.-M. *J. Electroanal. Chem.* **1987**, *227*, 299.
(34) Bard A. J.; Faulkner, L. *Electrochemical methods*; Wiley: New York, 1980.
(35) Kaufman, F. B.; Engler, E. M. *J. Am. Chem. Soc.* **1979**, *101*, 547.
(36) Dahms, H. *J. Phys. Chem.* **1968**, *72*, 362.
(37) Ruff, I.; Friedrich, V. J. *J. Phys. Chem.* **1971**, *75*, 3297.
(38) Buttry, D. A.; Anson, F. C. *J. Am. Chem. Soc.* **1983**, *105*, 685.
(39) Denny, R. A.; Sangaranarayanan, M. V. *J. Solid State Electrochem.* **1998**, *2*, 67.
(40) Sabater, M. J.; Corma, A. S.; Doménech, A.; Fornés, V.; García, H. *J. Chem. Soc., Chem. Commun.* **1997**, 1285.
(41) Doménech, A.; Formentín, P.; García, H.; Sabater, M. J. *Eur. J. Inorg. Chem.* **2000**, 1339.

(42) Formentín, P.; Folgado, J. V.; Fornés, V.; García, H.; Márquez, F.; Sabater, M. J. *J. Phys. Chem.* **2000**, *104*, 8361.
(43) Daum, P.; Lenhard, J. R.; Rolison, D.; Murray, R. C. *J. Am. Chem. Soc*. **1980**, *102*, 4649.
(44) Studies on intrazeolitic photochemical charge transfer for methylviologen and $Ru(bpy)_3^{2+}$ indicate that an efficient electron transfer coupled with recombination occurs at high guest loadings. See: (a) Sykora, M.; Kincaid, J. R.; Dutta, P. K.; Castagnola, N. B. *J. Phys. Chem. B* **1999**, *103*, 309. (b) Vitale, M.; Castagnola, N. B.; Ortins, N. J.; Brooke, J. A.; Vaidyalingam, A.; Dutta, P. K. *J. Phys. Chem. B* **1999**, *103*, 2408. (c) Yoon, K. B.; Park, Y. S.; Kochi, J. K. *J. Am. Chem. Soc.* **1996**, *118*, 12710.
(45) Lainé, P.; Lanz, M.; Calzaferri, G. *Inorg. Chem*. **1996**, *35*, 3514.
(46) Kerr, G. T. *Zeolites* **1983**, *3*, 295.
(47) Wietcamp, J., Karge, H. G., Pfeifer, H., Holderich, W., Eds. *Zeolites and Related Materials: State of the Art;* Elsevier: Amsterdam, 1994.
(48) Rolison, D. R. *Chem. Rev.* **1990**, *90*, 867.
(49) Baker, M. D.; Senaratne, C.; Zhang, J. *J. Chem. Soc., Faraday Trans*. **1992**, *88*, 3187.
(50) Barrer, R. M.; Klinowski, J. *J. Chem. Soc., Faraday Trans. I* **1972**, *68*, 1956.
(51) Barrer, R. M.; Klinowski, J. *J. Chem. Soc., Faraday Trans. 1* **1972**, *68*, 1956.